

A. SMALCERZ*[#], B. OLEKSIAK**, G. SIWIEC**

THE INFLUENCE A CRUCIBLE ARRANGEMENT ON THE ELECTRICAL EFFICIENCY OF THE COLD CRUCIBLE INDUCTION FURNACE

WPLYW KONSTRUKCJI TYGLA NA SPRAWNOŚĆ ELEKTRYCZNĄ PIECA Z ZIMNYM TYGLEM

A big interest in application of cold crucible furnace (CCF) for industrial, particularly metallurgical, processes has been observed in recent years. They are mainly utilised for melting of metal, glass and other materials. Analyses of processes that occur in such devices are performed; however, computer modelling is rarely applied. As a precise determination of the electromagnetic field distribution is essential for a proper analysis of processes in furnaces with cold crucibles, a complex 3D model development is necessary. In the paper, effects of a crucible design and current frequency on the efficiency of the induction furnace with cold crucible are presented. Numerical calculations were performed with the use of the Flux 3D professional software.

Keywords: induction heating, cold crucible furnace, simulation, electromagnetic field

W ostatnich latach piece z zimnym tygłem znajdują coraz szersze zastosowania w procesach przemysłowych szczególnie metalurgicznych. Wykorzystuje je się przede wszystkim do mieszania metali, szkła i innych materiałów. Wykonywane są analizy zjawisk zachodzących w tego typu urządzeniach, lecz tylko w nielicznych przypadkach wykorzystuje się modelowanie komputerowe. Wyznaczenie rozkładu pola elektromagnetycznego z należytą dokładnością to warunek niezbędny do właściwej analizy zjawisk zachodzących w piecach z zimnym tygłem i dlatego wymaga zbudowania skomplikowanego modelu 3D. W artykule przedstawiono wpływ konstrukcji tygla i częstotliwości prądu zasilającego na wydajność pieca z zimnym tygłem. Obliczenia numeryczne przeprowadzono z wykorzystaniem profesjonalnego programu komputerowego Flux 3D.

1. Introduction

A CCF provides an important method of semi-levitation melting of metals and other materials. It is used for processes involving highly reactive alloys (e.g. those of titanium or aluminium) as well as materials of high melting temperatures, such as molybdenum [1-9]. A typical characteristic of this process is lack of melted material contact with refractory materials and, thus, lack of its contamination. The process is conducted under the vacuum or inert (nitrogen, argon) conditions, which yields a high-purity material [10-12]. Due to electrodynamic forces, most of the alloy has no direct contact with the crucible. The part that has it creates a solidified layer which does not allow any direct contact of liquid metal with copper [13-17].

A view of a CCF is presented in Fig. 1. The basic element of the furnace is a water-cooled copper crucible (a cold crucible). There are also inductor coils and melted load in the furnace.

The inductor coil is supplied with alternating current which, due to electromagnetic induction, is a source of eddy currents in the crucible and melted load [18-19]. In order to ensure limited induction of eddy currents in the copper crucible, it is composed of several separated segments. Each segment is cooled with water. The segments are separated by thin layers of electrical insulator. Crucible cooling is also a reason for a solidified layer formation that does not allow any contact of the remaining material with the crucible wall. Moreover, the melted metal partly levitates due to Lorentz forces [20-24].

Procedures of designing and determining of a CCF parameters, such as the load, crucible and coil dimensions as well as the current intensity and frequency, are essential for the metal melting process. An experimental analysis of these parameters is difficult because it requires considering a lot of various factors. Numerical modelling of CCF processes allows understanding the effects of particular parameters as well as reducing the time and cost of investigational studies [25-28].

* SILESIAAN UNIVERSITY OF TECHNOLOGY, FACULTY OF MATERIAL SCIENCE AND METALLURGY, DEPARTMENT OF COMPUTER SCIENCE, 40-019 KATOWICE, 8 KRASIŃSKIEGO STR., POLAND

** SILESIAAN UNIVERSITY OF TECHNOLOGY, FACULTY OF MATERIAL SCIENCE AND METALLURGY, INSTITUT OF METALS TECHNOLOGY, 40-019 KATOWICE, 8 KRASIŃSKIEGO STR., POLAND

[#] Corresponding author: albert.smalcerz@polsl.pl

Physical processes that occur during induction heating are highly complex and interrelated. The electromagnetic field causes load heating and due to changing temperature, material properties and the load shape change which leads to changes in distribution of eddy currents, temperature and electromagnetic forces. The authors only focused on adequately precise determination of the electromagnetic field and omitted the temperature effects on the process. This approach ensures determination of the effects of the furnace design elements on its electrical efficiency. The process analysis requires development of a complex 3D model [29-31].

2. Study description

The research analysis is related to the system of a furnace with cold crucible, presented in Fig. 1. Due to the symmetry, the system constitutes 1/16 of the furnace. It consists of 1 segment of the water-cooled crucible, the load and a 14-coil inductor with a rectangular profile (Fig. 2). The basic dimensions are presented in Table 1.

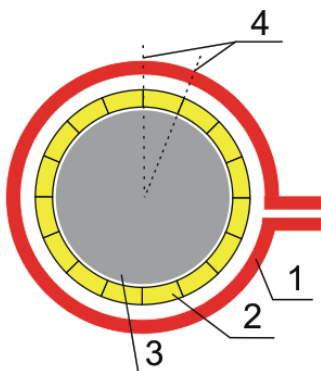


Fig. 1. View of a CCF: 1 – coil, 2 – crucible, 3 – load, 4 - axis symmetries

TABLE 1

Dimensions of the CCF used in the study (mm)

Crucible ID	Crucible OD	Coil ID	Coil OD	Load OD	Crucible Height CH	Load Height LH
49	64; 70; 76	69; 75; 81	75; 81; 87	42	120	200

Figures 2, 3 and Table 1 present the basic dimensions and material properties

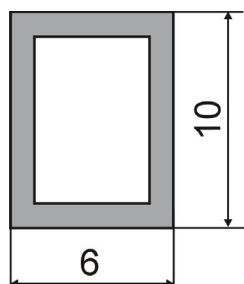


Fig. 2. Dimensions (in mm) of the inductor coil of the heater

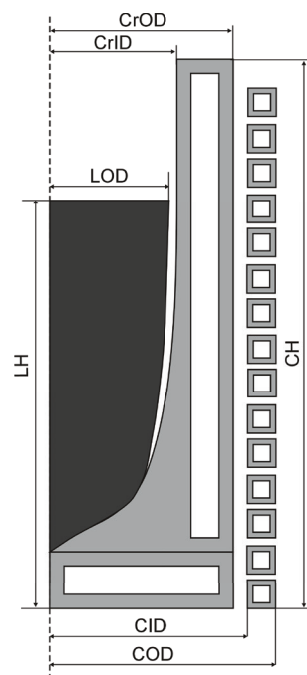


Fig. 3. Symbols of dimensions of induction heater

Table 2 presents material properties of particular elements of the heating system

TABLE 2

Material properties

parameter	unit	quantity
Load		
resistivity	(Ωm)	$\rho_0 = 2.82 \times 10^{-8}$
relative magnetic permeability	(-)	1
Crucible, inductor		
resistivity	(Ωm)	$\rho_0 = 1.72 \times 10^{-8}$
relative magnetic permeability	(-)	1

The system does not contain any ferromagnetic components ($\mu_r = 1$ in all cases). The discretization network for the magnetic field is composed of about 100,000 elements. The calculation time for one variant is approximately 10 hours.

3. Description of the model

To solve the eddy-current problems in three-dimensional systems, the $T\Phi-\Phi/\Phi_r$ model was used. It combines the electric vector potential T and scalar magnetic potential Φ for conductive areas (both magnetic and non-magnetic) with Φ formulated for non-conductive magnetic areas and reduced scalar magnetic potential Φ_r for non-conductive and non-magnetic areas [32-35].

The electric vector potential is defined by the formula

$$J = \text{curl } T \tag{1}$$

The scalar magnetic potential Φ is described by the dependence

$$\mathbf{H} = \mathbf{T} - \text{grad} \Phi \quad (2)$$

The above dependences lead to the equations which take the following form for harmonic quantities:

- for conductive areas

$$\text{curl}\left(\frac{1}{\gamma} \text{rot} \mathbf{T}\right) - \text{grad}\left(\frac{1}{\gamma} \text{div} \mathbf{T}\right) + j\mu\omega(\mathbf{T} - \text{grad} \Phi) = 0 \quad (3)$$

$$\text{div}[\mu(\mathbf{T} - \text{grad} \Phi)] = 0 \quad (4)$$

where

$\text{grad}\left(\frac{1}{\gamma} \text{div} \mathbf{T}\right)$ represents an expression referring to the

boundary condition $\text{div} \mathbf{T} = 0$,

- for non-conductive areas such as magnetic areas

$$\text{div}[\mu(-\text{grad} \Phi)] = 0, \quad (5)$$

while for the non-magnetic areas

$$\text{div}[\mu_0(-\text{grad} \Phi_r + \mathbf{H}_0)] = 0. \quad (6)$$

Fig. 4 presents the arrangement used for the numerical modelling. It consists of the load (red), inductor (black), copper crucible (yellow), thermal insulation, cooling (green) and solid skull.

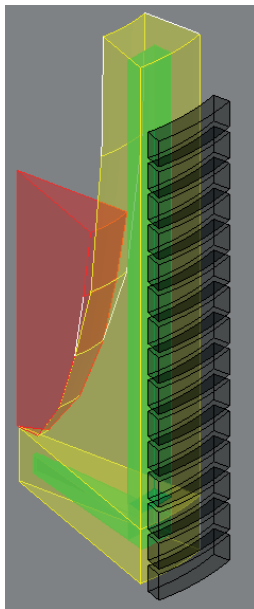


Fig. 4. The calculation model

4. Simulations of CCF

In the study, a finite element electromagnetic model of the CCF was developed using Flux 3D. To simplify the model, only a 1/16 of the system was modelled. A periodicity boundary condition was applied to the both sides (axis symmetries on Fig. 1). For those boundary conditions,

the mesh nodes on each side must be the same. To obtain the total power of the whole furnace, the results from one segment had to be multiplied by the number of segment. Aluminium was used as the load. Fig. 3 shows the one segment used in 3D simulation of the CCF. The air regions are not shown.

The study consisted of three cases:

1. The first analysed case was a change in the current frequency (5, 10, 20 kHz);
2. The next experiment was conducted for a various number of segments (6, 8, 12, 16);
3. The last analysed case was assessment of the crucible thickness (15, 21, 27 mm).

In Table 3, numbers of the calculation variants are presented.

TABLE 3

Cases of calculations

No. of variants	Frequencies, kHz	Number of segments	Thickness of crucible, mm
1	5	16	21
2	10	16	21
3	20	16	21
4	10	6	21
5	10	8	21
6	10	12	21
7	10	16	15
8	10	16	27
9	10	6	15
10	10	8	15
11	10	12	15

A constant current of 400 A was applied to the coil in all cases.

5. Results and discussion

Results of calculations for the aluminium heating and melting processes in the CCF are presented below. The analysis was limited to determine the magnetic field distribution in the system and Joule losses in the furnace parts. A model of CCF is presented in Fig. 4. All the calculations were performed for the constant current (400 A). The simulations differed in crucible design parameters and current frequencies.

During the numerical calculations, Joule losses in all

parts of the furnace were also controlled. Results for all crucible parts are presented in Table 4. The efficiency was determined using equation 7.

$$\eta = \frac{P_m}{P_c + P_i + P_m} \cdot 100\%. \quad (7)$$

TABLE 4
Joule losses generated in the elements of the CCF

Variant	P_{c_s} , W (crucible)	P_{i_s} , W (inductor)	P_{m_s} , W (melt)	η , %
1	3719.7	1441.3	473.6	8.4
2	4561.9	1820.2	606.7	8.7
3	5248	2083.8	760.3	9.4
4	2168.6	1029.1	391.7	10.9
5	2950.4	1730.6	538.9	10.3
6	3991.7	1797.1	591.4	9.3
7	4259.8	1692.2	642.6	9.7
8	4541.4	1641	586.2	8.7
9	2027.5	864	389.8	11.9
10	2777.6	1596.2	537.6	11
11	3657.6	1639.7	591.4	10.1

In Fig. 5, a graphic interpretation of the calculation results for the experiment 1 (current frequency changes – variants 1, 2, 3) is also presented. The frequency increase results in a slightly higher electrical efficiency of the system (approx. 1%) and a considerably increased power in the load (approx. 60%).

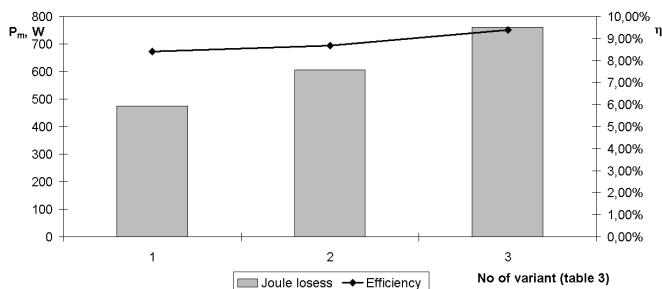


Fig. 5. Power in the load versus furnace efficiency depending on the current frequency

Fig. 6 present the effects of crucible segment number on the furnace efficiency and power in the metal. The analysis was performed for the furnace with 6, 8, 12 and 16 segments and for two crucible thickness values: 15 mm (variants 7, 9, 10, 11) and 21 mm (variants 2, 4, 5, 6). Reduction in the segment number results in increased electrical efficiency (about 2%) and decreased power in the melted metal (about 40%).

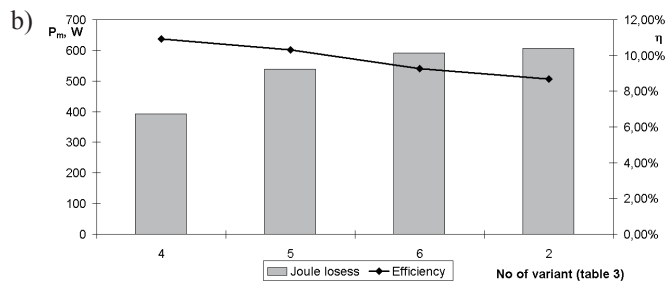
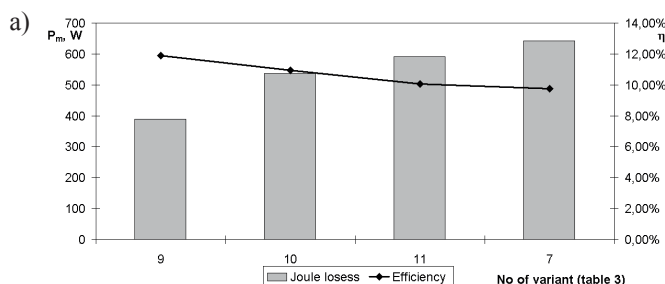


Fig. 6. Power in the load versus furnace efficiency depending on the crucible segment number; a) crucible thickness 15 mm, b) crucible thickness 21 mm

The last analysed parameter was the crucible thickness (variants 2, 7, 8 – Fig. 7). A thinner crucible leads to higher efficiency (about 1%) with a slightly increased power in the melted metal (approx. 10%).

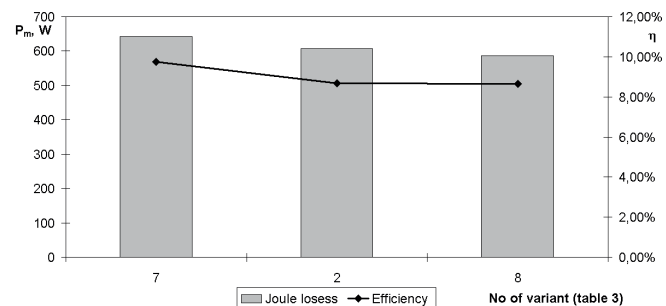


Fig. 7. Power in the load versus furnace efficiency depending on the crucible thickness

6. Conclusions

In the paper, a mathematical model of aluminium melting in a CCF is presented. Due to its complexity and structure, a 3D model is analysed with several simplifying assumptions and without considering the effects of melted metal flow. The most significant result of this kind of modelling is optimisation of both the system and the design of the crucible in order to obtain optimal heating conditions (i.e. total efficiency, particularly for metals of good electrical conductivity, e.g. copper, aluminium).

The analysis results show that the crucible design affects efficiency of the CCF. Both the crucible thickness and the segment number change the power in metal and the furnace electrical efficiency. The 3 performed series have led to the following conclusions:

- The frequency increase results in a slightly higher system efficiency (approx. 1%) and a considerably increased power in the load (approx. 60%).
- Reduction in the segment number results in increased electrical efficiency (about 2%) and decreased power in the melted metal (about 40%).
- A thinner crucible leads to its higher efficiency (about 1%) with a slightly increased power in the melted metal (approx. 10%).

REFERENCES

- [1] A. Fornalczyk, S. Golak, R. Przyłucki, Arch Civ Mech Eng **15**, 171-178 (2015).
- [2] A. Szkliniarz, W. Szkliniarz, Sol St Phen **176**, 139-148 (2011).
- [3] M. Koziol, A. Bogdan-Wlodek, J. Myalski, J. Wieczorek, Pol J Chem Technol **13**, 21-27 (2011).
- [4] J. Barglik, D. Dolega, A. Smagor, Magnetohydrodynamics **46**, 387-392 (2010).
- [5] W. Szkliniarz, A. Szkliniarz, Sol St Phen **197**, 113-118 (2013).
- [6] S. Golak, R. Przyłucki, J. Barglik, Arch Metall Mater **59**, 287-292 (2014).
- [7] R. Michalik, A. Tomaszewska, H. Woznica, Defect Diffus Forum **326-328**, 547-554 (2012).
- [8] A. Fornalczyk, S. Golak, M. Saturnus, Math Probl Eng ID 461085 (2013).
- [9] M. Koziol, J. Wieczorek, A. Bogdan-Wlodek, J. Myalski, J Compos Mater **47**, 2309-2319 (2013).
- [10] J.S. Becker, H.J. Dietze, Int J Mass Spectrom **228**, 127-150 (2003).
- [11] G. Siwiec, B. Oleksiak, A. Smalcerz, Arch Metall Mater **58**, 193-195 (2013).
- [12] H. Jacobi, Stahl Eisen **114**, 45-56 (1994).
- [13] D. Gombert, J. Richardson, A. Aloy, D. Day, Waste Management **02**, 24-28 Tucson (2002).
- [14] T. Wegrzyn, J. Piwnik, R. Wieszala, D. Hadrys, Arch Metall Mater **57**, 679-685 (2012).
- [15] J. Barglik, I. Dolezel, P. Karban, B. Ulrych, Compel **24**, 251-260 (2005).
- [16] T. Wegrzyn, J. Piwnik, Arch Metall Mater **57**, 539-543 (2012).
- [17] F. Bickford, C.C. Herman, D.K. Peeler, D. Gombert, J. Richardson, R. Goles, J.D. Vienna, A. Aloy, S. Stefanovsky, WSRC, South Carolina 2003.
- [18] A. Smalcerz R. Przyłucki, Int J Thermophys **34**, 667-679 (2013).
- [19] A. Glowacz, Arch. Acoust. **39**, 189-194 (2014).
- [20] A. Umbrasko, E. Baake, B. Nacke, A. Jakovics, HES-07, 277-292 Padova (2007).
- [21] E. Westphal, A. Muiznieks, A. Muhlbauer, IEEE T Magn **32**, 1601-1604 (1996).
- [22] I.V. Shurygina, Y.A. Polonskii, I.F. Masover, B.P. Aleksandrov, V.I Dobrovolskaya, V.M. Byndin, Refractories-USSR **22**, 622-627 (1981).
- [23] K. Kainuma, T. Take, M. Fujita, S. Hayashi, Stud Appl Electromag **13**, 753-756 (1998).
- [24] A. Morita, H. Fukui, H. Tadano, S. Hayashi, J. Hasegawa, M. Niinomi, Mat Sci Eng A-Struct **280**, 208-2013 (2000).
- [25] K. Pericleous, V. Bojarevics, R.A. Harding, M. Wickins, The third International Conference on CFD in the Minerals and Process Industries, 599-606 (2003).
- [26] A. Umbrasko, E. Baake, B. Nacke, Korus 2005, Proceedings, 372-376 (2005).
- [27] IV. Pozniak, AY. Pechenkov, AN. Schatunov, Compel **27**, 359-368 (2008).
- [28] E. Baake, B Nacke, F. Bernier, M. Vogt, A. Muhlbauer, Compel **22**, 88-97 (2003).
- [29] M. Niklewicz, A. Smalcerz, A. Kurek, Prz Elektrotechniczn **84**, 219-224 (2008).
- [30] J. Barglik, A. Smalcerz R. Przyłucki, J Comput Appl Math **270**, 231-240 (2014).
- [31] A. Smalcerz, R. Przyłucki, Metalurgija **52**, 223-226 (2013).
- [32] A. Candeo, C. Ducassy, P. Bocher, F. Dughiero, IEEE T Magn **47**, 918-921 (2011).
- [33] A. Smalcerz, Arch Metall Mater **58**, 203-209 (2013).
- [34] K. Kurek, DM. Dolega, Int J Mater Prod Tec **29**, 84-102 (2007).
- [35] M. Niklewicz, A. Smalcerz, Prz Elektrotechniczn **86**, 333-335 (2010).

Received: 20 October 2014.

